Heat Transfer Engineering

ISSN: 0145-7632 (Print) 1521-0537 (Online) Journal homepage: https://www.tandfonline.com/loi/uhte20

Fouling in a Steam Cracker Convection Section Part 1: A Hybrid CFD-1D Model to Obtain Accurate Tube Wall Temperature Profiles

Pieter Verhees, Abdul Rahman Akhras, Kevin M. Van Geem & Geraldine J. Heynderickx

To cite this article: Pieter Verhees, Abdul Rahman Akhras, Kevin M. Van Geem & Geraldine J. Heynderickx (2020) Fouling in a Steam Cracker Convection Section Part 1: A Hybrid CFD-1D Model to Obtain Accurate Tube Wall Temperature Profiles, Heat Transfer Engineering, 41:2, 127-137, DOI: 10.1080/01457632.2018.1522081

To link to this article: https://doi.org/10.1080/01457632.2018.1522081

Accepted author version posted online: 19 Sep 2018.
Published online: 04 Jun 2019.

HEAT TRANSFER ENGINEERING
2020, VOL. 41, NO. 2, 127–137
https://doi.org/10.1080/01457632.2018.1522081

Taylor & Francis
Taylor & Francis Group

Fouling in a Steam Cracker Convection Section Part 1: A Hybrid CFD-1D Model to Obtain Accurate Tube Wall Temperature Profiles

Pieter Verhees[a], Abdul Rahman Akhras[b], Kevin M. Van Geem[a], and Geraldine J. Heynderickx[a]

[a]Laboratory for Chemical Technology, Ghent University, Gent, Belgium; [b]Saudi Aramco Oil Company, R&D Center, Dhahran, Saudi Arabia

ABSTRACT

To study fouling in steam cracker convection section tubes, accurate tube wall temperature profiles are needed. In this work, tube wall temperature profiles are calculated using a hybrid model, combining a one-dimensional (1D) process gas side model and a computational fluid dynamics (CFD) flue gas side model. The CFD flue gas side model assures the flue gas side accuracy, accounting for local temperatures, while the 1D process gas side model limits the computational cost. Flow separation in the flue gas side at the upper circumference of each tube suggests the need for a compartmentalized 1D approach. A considerable effect is observed. The hybrid CFD-1D model provides accurate tube wall temperature profiles in a reasonable simulation time, a first step towards simulation-based design of more efficient steam cracker convection sections.

Introduction

Worldwide the high demand for fossil fuels is depleting the conventional oil reserves. Switching to alternative oil reserves or enhanced oil recovery methods changes the characteristics of the recovered oil. Mostly, the alternative oil reserves contain more impurities such as heavy metals, sulfur, nitrogen, and polyaromatic components, while they also have a higher final boiling point (FBP) [1–3]. Processing these heavy oil fractions results in fouling of equipment both in upstream and downstream applications [4, 5].

In steam cracking—the predominant process to make ethylene, propylene and many more valuable chemical building blocks—the use of heavier hydrocarbon feeds is thus economically driven, but increased equipment fouling is observed. In the radiant section of a steam cracker, where tubular reactors are suspended in a fired furnace, coke deposition on the reactor wall is an all-time phenomenon, and its effect on operation has been studied in detail [6]. Fouling in the convection section of a steam cracker, a series of horizontal tube heat exchangers, becomes unavoidable due to the high(er) FBP and to the increase of polyaromatic compounds, such as asphaltenes and resins, in the feed [7, 8]. To mitigate and more preferably prevent fouling, established steam cracker furnace and convection section designs have to be reconsidered. The current study focuses on fouling in the heat exchangers in the convection section.

Figure 1 shows the complete steam cracker and zooms in on the convection section, where the feed is prepared for cracking in the reactor tubes in the radiant section. The different heat exchangers, using the heat in the flue gas coming from the radiation section, are named. A liquid feed is partially evaporated in the top bank, the evaporator. The vapor/liquid flow is then mixed with overheated steam, coming from the steam overheater, in the steam dilution injector (SDI) (Figure 1). For a conventional liquid feed, this steam dilution suffices to complete the feed evaporation. In the bottom banks, named mixture overheaters (or high temperature coils, i.e. HTC), the hydrocarbon/steam mixture is heated to the required reactor tube inlet temperature. When cracking feeds with a high(er) FBP, the heavy tail of the feed has not yet completely evaporated when leaving the SDI. As a consequence, a spray flow containing small droplets of heavy hydrocarbons enters the HTCs. Droplets that

CONTACT Professor Geraldine J. Heynderickx geraldine.heynderickx@ugent.be Laboratory for Chemical Technology, Ghent University, Technologiepark 914, B-9052 Gent, Belgium.
Color versions of one or more of the figures in the article can be found online at www.tandfonline.com/uhte.

Nomenclature

1D	One-dimensional
3D	Three-dimensional
c_p	Specific heat, J/(kg K)
d	Diameter, m
EVAPH	Evaporator
FBP	Final boiling point
HTC	High temperature coils
h	Heat transfer coefficient, W/(m^2 K)
k	Turbulent kinetic energy, m^2/s^2
K	Watson characterization factor, dimensionless
$\dot{m}$	Mass flow rate, kg/s
Nu	Nusselt number, dimensionless
PIONA	Content of paraffins, isoparaffins, olefins, napthenes and aromatics of oil feed, wt%
Pr	Prandtl number, dimensionless
q	Heat flux, W/m^2
RANS	Reynolds-Averaged Navier–Stokes equation
Re	Reynolds number, dimensionless
RSM	Reynolds Stress Model
SDI	Steam dilution injector
T	Temperature, K
U	Overall heat transfer coefficient, W/(m^{2}K)
z	Axial position, m

Greek symbols

ε	Turbulent dissipation rate, m^2/s^3
κ	Thermal conductivity, W/(m K)
γ	Angular coordinate, radian
θ	Compartment angle, radian

Subscripts

b	bulk
i	inner
j	integer
o	outer

impact on the tube wall experience the effect of high tube wall temperatures, resulting in tube fouling by coke formation [7, 8].

Fouling is reported to occur mainly in the high temperature banks downstream the SDI. Mahulkar et al. [8] reported that the extent of fouling is highly influenced by the tube wall temperatures. These wall temperatures influence both the droplet impingement behavior and the fouling layer growth. The tube wall temperatures of all heat exchangers can only be accurately determined by a coupled simulation of flue gas and process gas side of the steam cracker convection section. In the present study a coupled simulation of flue gas and process gas side is performed.

The first reported coupled simulation of a steam cracker convection section was performed by De Schepper et al. [9], simulating the convection section presented in Figure 1. De Schepper et al. [9] developed a complete three-dimensional (3D) computational fluid dynamics (CFD) convection section model that enables the detection of hot spots on the tube walls, possibly resulting in local increased fouling. Almost a decade later, Hu et al. [10] applied this model to a more complex convection section, with an increased number of steam overheaters, aiming at an increased thermal efficiency. Verhees et al. [11] significantly decreased the computational cost of a coupled simulation by the development of a one-

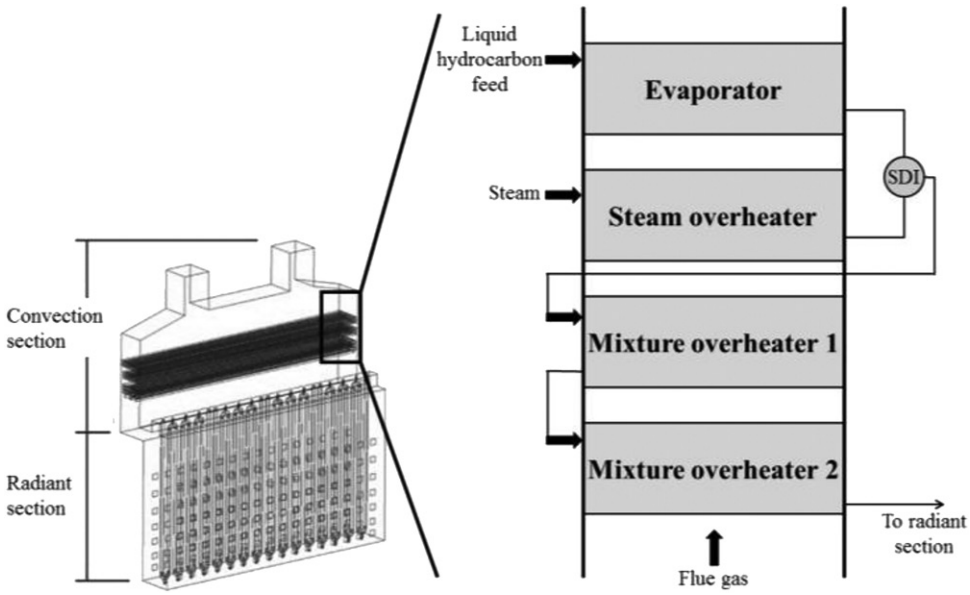

Figure 1. Schematic of a typical steam cracker and convection section.

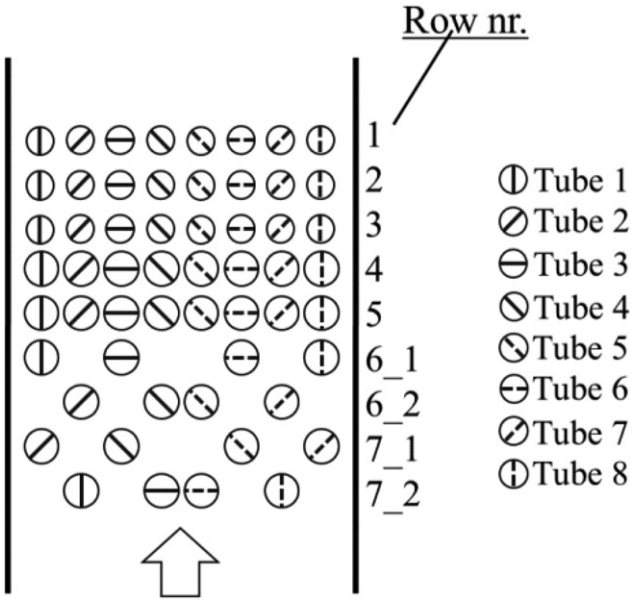

Figure 2. Configuration of HTC-1 (rows 1–3) and HTC-2 (rows 4–7).

dimensional (1D) convection section model. The decrease in computational time comes at the cost of loss of simulation detail for the temperature profiles. Choosing between a 1D and a 3D CFD model is thus a tradeoff between level of simulation detail and computational cost. In this study, both CFD modeling and 1D modeling are combined in a hybrid model to gain in computational time but retain sufficient simulation detail for local temperature profiles. The process gas side is simulated using a 1D model. A CFD model captures the flue gas flow phenomena.

Case

The geometry and the operating conditions in the present study are both taken from De Schepper et al. [9]. The convection section, schematically depicted in Figure 1, contains four banks, i.e. an evaporator (EVAPH), a steam overheater, and two mixture overheaters (HTC-1 and HTC-2), and a SDI.

The present study focuses on the HTC-1 and HTC-2, where fouling is most likely to occur. The combined banks consist of eight tubes, each tube making seven passes through the flue gas box (Figure 2). The tube passes in HTC-1 (rows 1–3) have an inline configuration. A mixed inline and staggered configuration is adopted for HTC-2 (rows 4–7). The last tube pass in HTC-2 is shifted one position to the right or left, to ensure a more equal heat distribution over the tubes (Figure 2). The main geometrical parameters of both banks are listed in Table 1.

Table 1. Geometry details of HTC-1 and HTC-2.

		HTC-1	HTC-2
Inner diameter	*m*	0.07	0.1
Wall thickness	*m*	0.005	0.005
Horizontal pitch	*m*	0.14	0.14
Vertical pitch	*m*	0.15	0.204
Length tubes	*m*	11.38	11.38

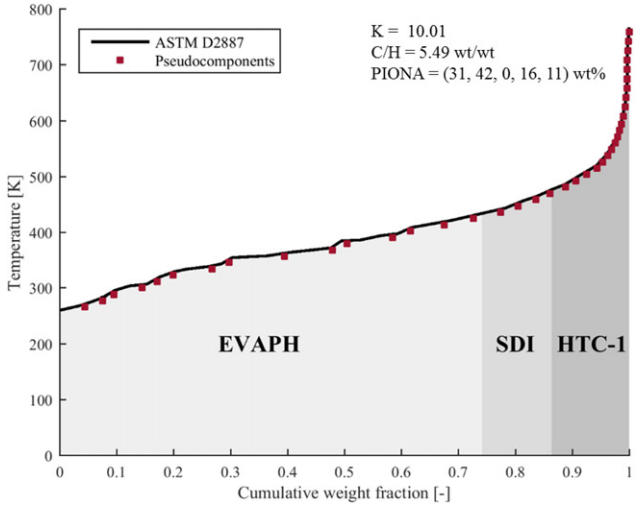

Figure 3. Simulated distillation curve of the gasoil represented by 40 pseudocomponents (■).

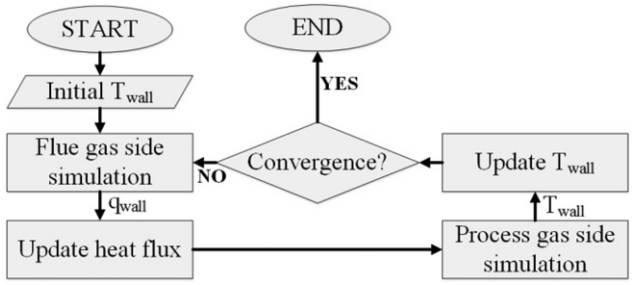

Figure 4. Iterative procedure for the coupled simulation of flue gas and process gas side of the convection section.

Heat is provided by the hot flue gas coming from the furnace. The flue gas enters at the bottom of the convection section and flows in opposite direction as compared to the process gas flow direction. Flue gas enters the convection section at 1450 K and 1 bar with a mass flux of 1.41 kg/(m^{2}s). The flue gas is composed of the typical combustion products, namely 72.5 wt% N_2, 2.6 wt% O_2, 13.3 wt% CO_2 and 11.6 wt% H_2O.

The gasoil feed is a complex hydrocarbon mixture consisting of over a thousand components. The thermal behavior of the complete gasoil was found to be accurately described when it is replaced by 40 pseudocomponents [12]. The gasoil is characterized by a simulated distillation curve, the Watson characterization factor K, the paraffins, iso-paraffins, olefins,

napthenes and aromatics content (PIONA) and the C/H ratio, listed in Figure 3.

Based on the work by De Schepper at al. [13] the vapor quality of the feed leaving the evaporator is calculated to be 0.7. An energy balance over the SDI learns that the vapor quality rises to 0.86 when mixing the partially evaporated feed with steam of 600 K. The liquid hydrocarbons enter HTC-1 as droplets entrained in the vapor phase. It is assumed that the evaporated part of the feed consists of the lower boiling components, while the droplets are made up of higher boiling components only. From the distillation curve the temperature at the inlet of HTC-1 is determined to be 526 K. The gasoil/steam mixture mass flow rate of 8.8 kg/s is equally distributed over the eight tubes of HTC-1. The steam-to-oil ratio is 1 kg_{steam}/kg_{HC}.

For more details on the configuration and operating conditions reference is made to De Schepper et al. [9].

Methodology

Coupling procedure

In the convection section, heat is transferred from the flue gas side to the process gas side. Flue gas side and process gas side are modeled using a CFD model and a 1D model, respectively. CFD flue gas side simulations are performed with imposed outer tube wall temperatures for each tube pass as boundary condition. Process gas simulations are performed with imposed heat fluxes along each tube pass as boundary condition. Outer tube wall temperatures are updated as a result of a process gas side simulation, while heat fluxes are updated as a result of a flue gas side simulation. The iterative procedure of the coupled simulation is shown in Figure 4.

The combined two banks, HTC-1 and HTC-2, consist of 8 tubes making in total 56 tube passes. The convergence of this complex coupled problem is not guaranteed. To ensure convergence, a row-wise update of the boundary conditions (temperatures and heat fluxes) is adopted, starting from the bottom row where the flue gas enters the convection section, following the flow of the flue gas to the top. To further increase the stability of the coupled simulation procedure, under-relaxation is applied.

In total, 200 iterations are required to obtain convergence, calculating for 4 days on an eight core machine. Convergence is reached when the relative difference of the heat flux between the previous and the current iteration for each tube pass is lower than 4%.

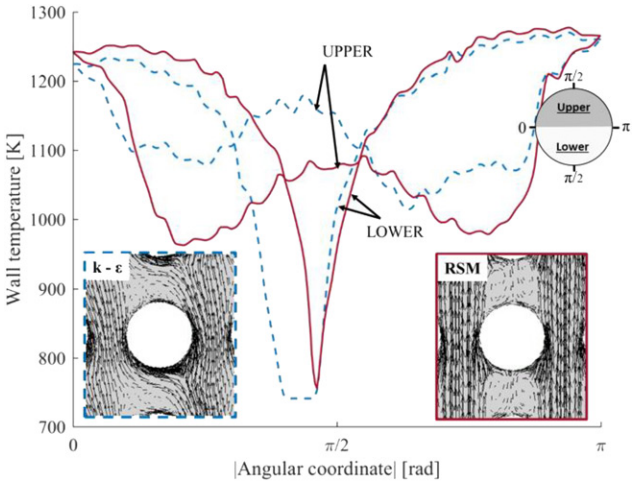

Figure 5. Circumferential tube wall temperature profile for tube 4 (—), row 3 of HTC-1 combined with vector plot of the flue gas flowing over the tube. $k-\varepsilon$ (⦸) and RSM (- - -) turbulence modeling. Imposed uniform heat flux of 30 kW/m^2.

Flue gas side

Model

The flue gas side is modeled using the CFD approach developed by De Schepper et al. [9]. The main consideration is the level of detail of the applied turbulence model to close the Reynolds-Averaged Navier–Stokes (RANS) equations. The k–ε turbulence model, used by De Schepper et al. [9] and Hu et al. [10], provides efficient closure of the RANS equations by applying the Boussinesque approximation, assuming isotropic eddies. In a close *staggered* packing of tubes, this assumption is valid as the dense packing of tubes neutralizes the highly isotropic vortex shedding, often observed for crossflow over tube arrays [14]. However, the k–ε model mostly fails for flow over an *inline* packing of tubes (rows 1–5). Vortex formation in the wake of a tube is likely but will not be captured by the k–ε model. Vortex formation is captured when applying the Reynolds Stress Model (RSM) [15]. The increase in hydrodynamics detail for the flue gas flow comes at an increase of the computational cost by a factor of 2–3. As illustrated by Figure 5, a change in the flue gas hydrodynamics results in a remarkable change of the circumferential tube wall temperature profiles. The temperature profiles are obtained with an imposed heat flux of 30 kW/m^2. In this work, CFD modeling of the flue gas side using RSM is thus required.

Finally, the thermal boundary layer around the tubes is directly solved by using a very thin mesh at

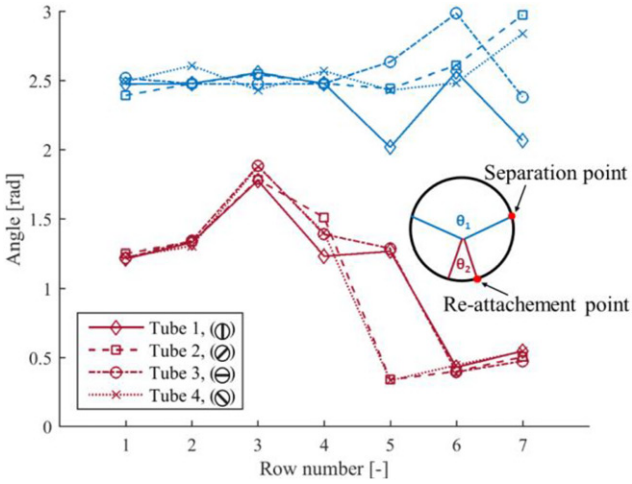

Figure 6. Angle of compartments of the tube passes, (top) θ_1 and (bottom) θ_2, of tube 1 (◇), tube 2 (□), tube 3 (◯) and tube 4 (×).

the tube wall. This enables to calculate the steep velocity and temperature gradients at the tube wall required for accurate heat transfer results.

Radiation, mainly from the hot convection section walls, is significant for rows 5–7. However, the high computational cost accompanying radiation modeling, does not justify the small change in wall temperature of the tubes of interest, i.e. rows 1 and 2, when studying fouling.

Geometry

In the present study, the simulation domain is limited to the bottom two tube banks (HTC-1 and HTC-2) sensible to fouling. Hence, the simulated domain contains 56 tube passes. To limit the computational cost, the CFD calculations are reduced to a 2D problem by assuming the flue gas temperature to be constant along the length of the tubes. A mesh selectivity study is performed. The mesh contains 1.2 million cells, including mesh refinement around the tube walls to calculate the thermal boundary layer around the tubes.

Process gas side

Model

The process gas side of the convection section is modeled using the model recently introduced by Verhees et al. [11]. Based on the study of Mahulkar et al. [8], it is assumed that droplets suspended in the vapor flow deposit in the first, adiabatic bend of HTC-1. Hence, the local heat and mass transfer effect of the small portion of liquid percolating in the heated tubes and evaporating is not accounted for in the present study. The fluid temperature in the HTC tubes is calculated by solving the discretized single phase, steady state energy balance along the tubes:

$$\dot{m}\ d\left(c_p T_\mathrm{b}\right) = q_\mathrm{wall}\pi d_o dz \tag{1}$$

with $\dot{m}$ the total mass flow, c_p the specific heat, z the axial coordinate, d_o the outer diameter and q_wall the imposed heat flux calculated from the flue gas side simulation. q_wall is the boundary condition for the process gas side simulation. The outer tube wall temperature, boundary condition for the flue gas side simulations, is updated using the following equation:

$$T_\mathrm{wall} = \frac{q_\mathrm{wall}}{U} + T_\mathrm{b} \tag{2}$$

with T_b the calculated fluid bulk temperature. The overall heat transfer coefficient from outer wall to fluid, U, is the sum of the thermal resistance of the tube wall and the fluid flow:

$$\frac{1}{U} = \frac{1}{h}\frac{d_o}{d_i} + \frac{d_0}{2\kappa}\ln\frac{d_o}{d_i} \tag{3}$$

with d_i and d_o the inner and outer diameter of the tube, h the heat transfer coefficient and κ the thermal conductivity of the tube wall.

The thermal conductivity, κ, is assumed constant and is given a value of 35 W/(m K). Accurately predicting the heat transfer coefficient h is the main challenge when modeling the process gas side, in particular for two phase flow. At the inlet of the HTC-1 tubes, a spray flow is injected. In the present study the flow is assumed to be single phase flow. The heat transfer coefficient for single phase forced convection flow is calculated using the Dittus–Boelter correlation [16]:

$$Nu = 0.023Re^{4/5}Pr^{0.4} \tag{4}$$

with Re and Pr the Reynolds and the Prandtl number, respectively.

Crossflow of the flue gas over the HTC tubes results in flow separation at sufficiently high Reynolds numbers as observed in Figure 5. Flow separation results in the formation of a wake, made up of two vortices above each tube. In this wake, the flue gas velocity is an order of magnitude smaller than the bulk flue gas velocity. For the tubes in an inline configuration (rows 1–5), it is observed that a tube is positioned in the wake of the tube in the lower row (observed for rows 1–4). As a result, a low velocity region is formed around the lower zone of the tube (angle θ_2, Figure 6). The low flue gas velocity region results in a low heat transfer coefficient zone. At the end of this lower zone with limited flue gas velocity, the flue gas flow re-attaches to the tube. The high flue

gas velocity and corresponding shear sideways of the tubes result in a more efficient heat transfer. Finally, the flue gas separates from the tube wall. In the zone above the tube (angle θ_1, Figure 6), the above-mentioned wake is formed and the flue gas velocity and thus the heat transfer coefficient are low. Based on these observations, the tube in the 1D process gas side model is compartmentalized in three regions, i.e. a lower dead zone, a high shear side zone and an upper wake zone (Figure 6). In the compartmentalized approach, the heat flux q_{wall} is taken as the area-weighted average of the heat flux contributions of each compartment, as calculated from the flue gas side simulation:

$$q_{\text{wall}} = \sum_{j=1}^{3} \frac{q_{\text{wall},j}\theta_j}{2\pi} \tag{5}$$

with q_j and θ_j the heat flux and angle of compartment j. The heat exchanging area is proportional to the angles of the compartments, shown in Figure 6. Remark that the angles of the compartments differ for the different tubes and are strongly related to the configuration of the tube passes. The outer tube wall temperatures, boundary condition for the CFD flue gas simulations, are computed as:

$$T_{\text{wall},j} = \frac{q_{\text{wall},j}}{U} + T_{\text{b}} \tag{6}$$

in the compartmentalized approach.

Geometry

Details of the simulated tube banks HTC-1 and HTC-2 are listed in Table 1. Following a first discretization in the axial tube direction, the circumference of the tube wall is divided into three compartments if the compartmentalized approach is used. The angles of the different compartments are determined from the shear stress profile on the tube wall resulting from a preliminary flue gas side simulation. At the stagnation points—the flow re-attachment point and the flow separation point—the shear stresses on the tube wall are minimal. Based on the position of these minima, that is the position of the re-attachment and separation point, the angles θ_j are determined. Figure 6 learns that the lower compartment of a tube (θ_2) is negligible for the lower row of the tubes in an inline configuration (row 5) and the tubes in a staggered configuration (rows 6–7). The latter is due to the fact that the tubes in these rows are not positioned in the wake of a tube of a lower row, contrary to the tubes in rows 1–4, as discussed above. The angle of the compartments is thus strongly related to the flue gas velocity field.

Table 2. HTC-2 outlet hydrocarbon/steam mixture temperature.

Tube nr.	Outlet temperature	
	K	
	1D	1D compartmental
1	874	874
2	892	891
3	888	886
4	889	884
5	885	883
6	887	883
7	895	891
8	876	875
Average	886	883

Results

Hybrid CFD-1D model

Flowing over HTC-1 and HTC-2, the flue gas is calculated to cool down from 1450 K to 1279 K. The HTC-2 outlet hydrocarbon/steam mixture temperatures are listed up in Table 2. The outlet temperatures are calculated to be rather uniform over all eight tubes. The average HTC-2 outlet temperature, 886 K, is close to the typical industrial reactor inlet temperature (i.e. the HTC-2 outlet temperature) which is about 890 K [17].

As HTC-2 outlet temperature differences are less than 21 K, the total heat transfer to each tube is about constant. Tubes 2 and 7 have the highest outlet temperatures. This is, amongst other, a consequence of the configuration of the HTC-2, more specifically of the fact that, in row 5, tubes 2 and 7 are not positioned in the wake of a tube in row 6 (Figure 2). The lower tube area, with limited heat transfer for tubes 2 and 7, is thus very small. The latter is confirmed in Figure 6 where the θ values proportional to the size of the zones are compared for tubes 1, 2, 3 and 4. The value of θ_2 for tubes 1 and 3 is considerably larger than for tubes 2 and 4 in row 5. The lower velocities at the convection section walls result on the one hand in smaller upper zones with low heat transfer for tubes 1 and 8 and on the other hand in considerably less heat transfer to these outer tubes. It can be seen in Table 2 that this leads to low outlet temperatures of tubes 1 and 8.

Figure 7a shows the heat flux to each of the eight tubes in all seven rows. The above observations, describing the influence of θ_1, θ_2 and the vicinity of the wall, are confirmed. Additionally, the bottom rows 6 and 7 have a significantly smaller heat flux, even though the lower zone, that is the value of θ_2 (Figure 6) is smaller. The heat fluxes for rows 6 and 7 correspond to a lower interstitial flue gas velocity reducing the value of the convective heat transfer coefficient due to a lower Reynolds number. In Figure 7b, the heat flux profile, outer tube wall temperature profile

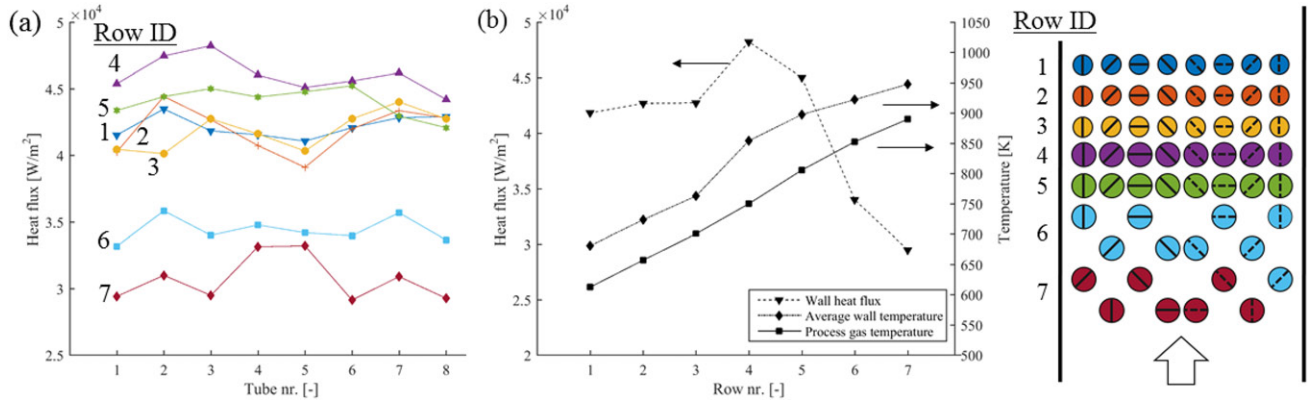

Figure 7. (a) Outer wall heat flux to each tube in different rows. (b) Heat flux, outer tube wall temperature and process gas profile for tube 3 throughout HTC-1 and HTC-2 obtained using the hybrid CFD-1D model.

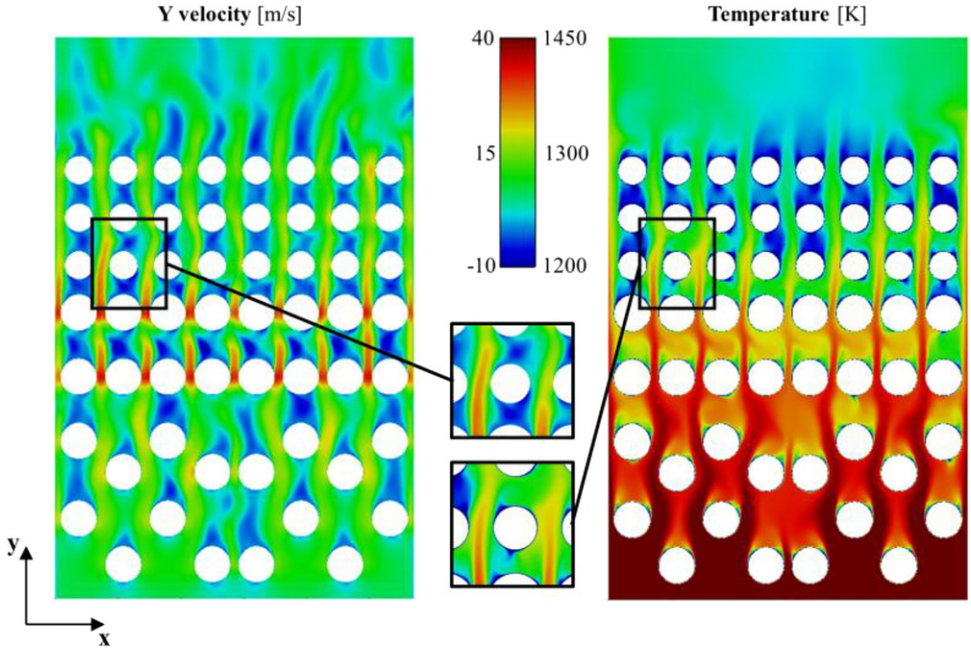

Figure 8. Contour plot of the flue gas axial velocity (left) and temperature (right).

and process gas temperature profile for tube 3 are presented. The low heat flux to the tube in row 3, last pass of HTC-1, corresponds to the larger lower dead zone, θ_2 (Figure 6). The latter is a consequence of the fact that the tubes in row 4, first pass of HTC-2, have a larger diameter, and thus a wide wake. Figure 7b also clearly shows that the difference between the wall and the bulk temperature is inversely proportional to the heat flux. The latter follows from Equation (2), where the overall heat transfer coefficient U is considered uniform over each cross-section of a tube.

Figure 8 shows the velocity and temperature contour plots of the flue gas and confirms the above made observations. The large dead zones with low flue gas velocity below and above the tubes result in lower local heat fluxes. This observation supports the need to compartmentalize the 1D simulation of the gas side process to refine the simulation results.

Finally it is observed that the results of the coupled simulation using the hybrid CFD-1D approach are symmetrical at the flue gas side of the convection section (Figure 8). This implies a possible further reduction in computational costs by imposing a symmetry boundary condition, with symmetry axes, separating tubes 4 and 5.

Hybrid CFD-1D compartmentalized model

The simulation is reconducted with the hybrid CFD-1D compartmentalized model. The outlet temperatures

of HTC-2 can be found in Table 2. They differ by no more than 5 K from the results of the hybrid CFD-1D model. Hence, the total heat transfer does not significantly differ. This conclusion is extended to the average heat flux per tube pass. The average wall heat flux does not significantly change switching from the hybrid CFD-1D to the CFD-1D compartmentalized model. This is confirmed by the parity plot of the (area-weighted) average heat flux per tube pass, shown in Figure 9. The same result is observed for the average wall temperature (not shown).

The subdivision of the tube into three compartments, based on the shear stress profile, is to account for the local variations in wall temperature and heat flux. Figure 10 shows the circumferential heat flux for tube 3 passing in rows 1, 3, 4, and 6. Similar profiles are computed for all tubes and rows, as expected. The upper and lower compartment, θ_1 and θ_2, are located around $\pi/2$. The lowest heat flux is observed in the upper compartment (θ_1). Hence, the wake originated by flow separation highly influences the heat transfer to the tube. Figure 10 also shows that in the compartmentalized approach the amplitude of the heat flux profiles slightly decreases. In practice, the main interest is the wall temperature profile of the tubes. In particular, the maximum wall temperature is important since this will be a measure for the onset of fouling. The flue gas CFD simulation yields a circumferential heat flux profile for each tube pass. Based on the heat flux profile, on the overall heat transfer coefficient and on the bulk temperature (obtained from the process gas side simulations), the corresponding circumferential tube wall temperature profile is extracted using the following equation:

$$T_{\text{wall}}(\gamma) = \frac{q_{\text{wall}}(\gamma)}{U} + T_{\text{b}} \tag{7}$$

with γ the angular coordinate. Mahulkar et al. [8] reported that the liquid droplets almost instantly deposit on the tube wall upon entering the HTC-1. Hence, the fouling layer will mainly develop in the tube passes of the top row(s) of HTC-1. In Figure 11, the wall temperature profiles for tube 3 in rows 1 and 3 are presented. The shape of these wall temperature profiles corresponds to the shape of the heat flux profiles. The relatively large difference between circumferential heat fluxes is flattened out to lower differences in wall temperatures as can be concluded from Eq. (7). The maximum wall temperatures occur at the lower part of the tubesides, as seen in Figure 11. This is a consequence of the high flue gas velocities and corresponding high heat fluxes.

Figure 12 compares the difference in maximum wall temperature and local bulk temperature for all 56 tube passes using both modeling approaches. Based

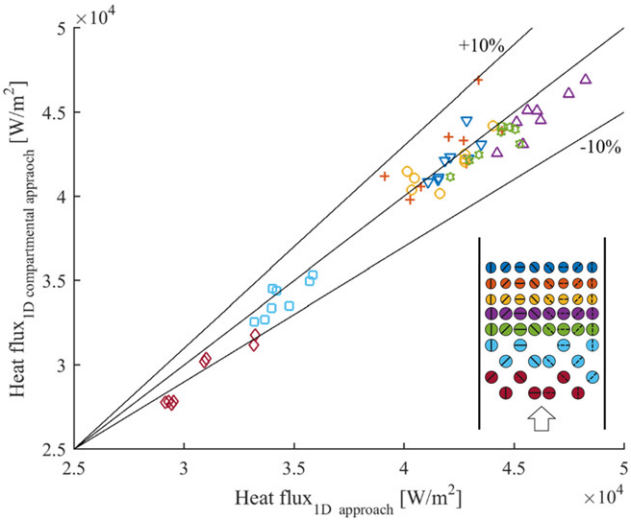

Figure 9. Parity plot of the average heat flux comparing the 1D with the 1D compartmentalized approach.

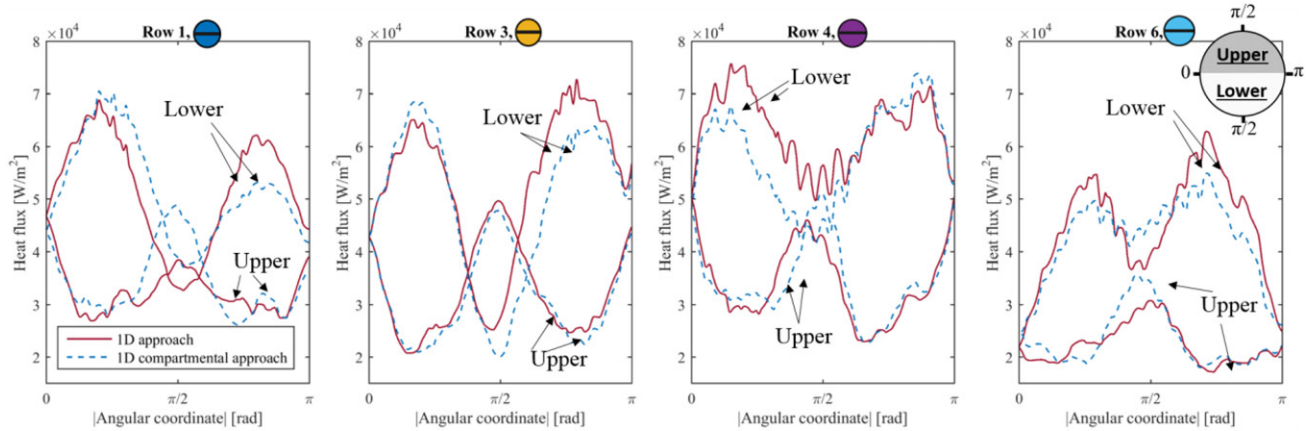

Figure 10. Heat flux profiles of tube 3 in rows 1, 3, 4 and 6 obtained by the 1D approach and the 1D compartmentalized approach.

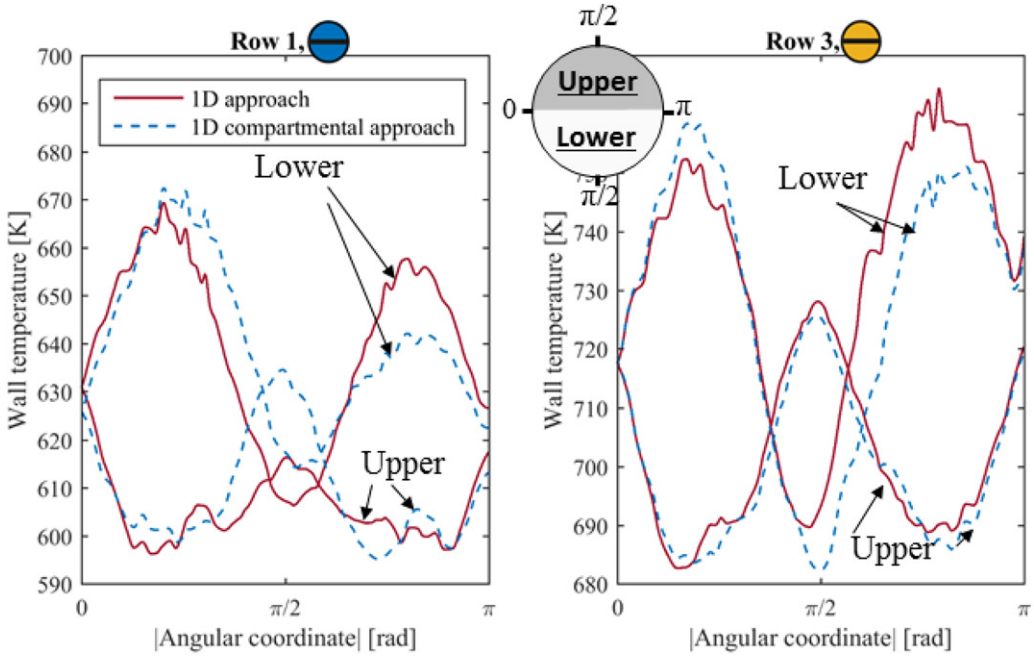

Figure 11. The wall temperature profiles of tube passes of tube 3 and rows 1 and 3.

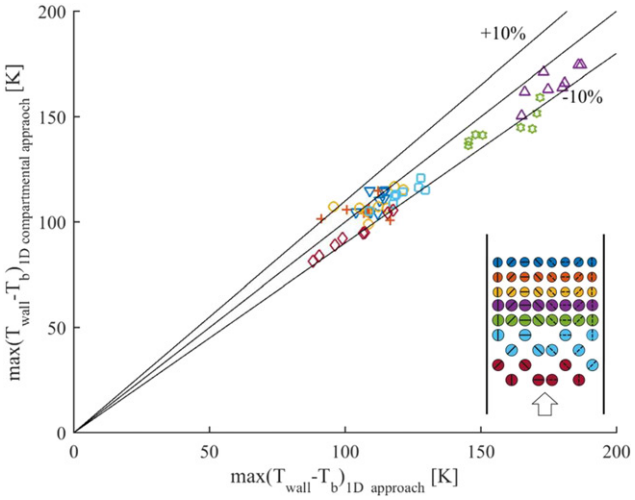

Figure 12. Parity plot of the difference between the maximum wall temperature and the bulk temperature for each tube pass comparing the 1D with the 1D compartmentalized approach.

on Eq. (7), this difference corresponds to the maximum heat flux scaled by the overall heat transfer coefficient, $q_{\text{wall, max}}/U$. The hybrid CFD-1D compartmentalized approach computes a lower maximum difference ($T_{\text{wall, max}} - T_{\text{b}}$) as compared to the hybrid CFD-1D approach. This corresponds well with the decrease in amplitude in wall heat flux profiles (Figure 10).

The maximum wall temperature difference between the 1D and 1D compartmentalized approach significantly differs in HTC-2. High gradients are present in the temperature and heat flux profiles, as seen in Figures 10 and 11. Hence, three compartments can be insufficient to accurately capture these profiles. Most possible, the wall temperature will further decrease when increasing the number of compartments. For instance, the left and right side of the tube pass (left and right of $\pi/2$ in Figure 11) are far from symmetrical, suggesting to account for additional compartments. Hence, a sensitivity study has to be performed to determine the number of compartments that has to be taken into account.

Conclusions

In this work, a coupled flue gas and tube side simulation of the convection section is performed. In order to obtain valuable tube wall temperature profiles in a reasonable amount of time a hybrid approach is chosen. The wall heat flux is obtained by the CFD simulation of the flue gas side. A 1D simulation of the tube side results in a wall temperature profile which is again passed to the CFD simulation. It is observed that a pure 1D model does not accurately capture local information. Based on the characteristics of the flue gas flow field, i.e. wake formation, the tube is divided in three compartments. A considerable effect on the results is observed. Compared to the pure 1D model, compartmentalization decreases ($T_{\text{wall, max}} - T_{\text{b}}$) by up to 10%. Given the effect of $T_{\text{wall, max}}$ on tube fouling, a compartmentalized approach is preferred.

Notes on contributors

Pieter Verhees is a PhD Candidate at the Laboratory for Chemical Technology (LCT) of Ghent University under the supervision of Prof. Van Geem and Prof. Heynderickx. In 2013 he earned a Master of Science degree in Chemical Technology at the LCT. After earning his master, he immediately started his PhD at the LCT. Currently he is studying fouling in the convection section of a steam cracker based on computational fluid dynamics simulations.

Abdul Rahman Akhras is currently working as a science specialist at the Research and Development Center of Saudi Aramco Oil Company. He holds a PhD degree in Fluid Dynamics from INSA-Lyon-France (Institut National des Sciences Appliquées de Lyon), October 2002. He then worked as a post-doctoral researcher at French Petroleum Institute-France (I.F.P) for 2 years. Before joining Saudi Aramco Oil Company, he worked as a Senior Project Engineer at Cril Technology Company-France for more than two years. He has authored and coauthored more than 25 scientific papers in international journals and conferences and has 16 US patents and 1 French patent. At R&D center of Saudi Aramco Oil Company, he managed several projects involving computational fluid dynamics as well as experimental fluid dynamics with many measurement techniques. Now he is focusing on research areas related to the thermal cracking of crude oil to chemical and to high severity fluid catalytic cracking.

Kevin Van Geem is a full professor and member of the Laboratory for Chemical Technology of Ghent University. Thermochemical reaction engineering in general and in particular the transition from fossil to renewable resources are his main research interests. He is a former Fulbright Research Scholar of MIT and directs the Pilot plant for steam cracking and pyrolysis. He is the author of more than hundred scientific publications and has recently started his own spin-off company. He is involved in on-line and off-line analysis of complex petrochemical and biochemical samples using comprehensive two-dimensional gas chromatography. Direct experimental scale-up, detailed kinetic modeling, process modeling (Aspen, ProII), and the role of additives belong to his expertise.

Geraldine Heynderickx is a senior full professor and member of the Laboratory for Chemical Technology (LCT) of Ghent University. Reactor hydrodynamics are the main lead in her research. Multiphase flow regimes are studied under varying conditions, comprising combustion, evaporation, thermal and catalytic reactions. Optimization of existing processes and development of new processes aim at process intensification. Computational fluid dynamics research is linked to handling fossil and renewable resources in different process technologies. She directs the Riser pilot setup and the Vortex pilot setup at the LCT. She has authored over 80 scientific publications. Numerical and experimental process and flow modeling, heat and mass transfer study under varying flow conditions belong to her main expertise.

References

[1] M. R. Riaze, "Characteristics of heavy fractions for design and operation of upgrading related processes," in Proc. AIChE Annual Meeting, San Francisco, CA November 7, 2013.

[2] R. G. Santos, W. Loh, A. C. Bannwart, and O. V. Trevisan, "An overview of heavy oil properties and its recovery and transportation methods," *Brazil. J. Chem. Eng.*, vol. 31, no. 3, pp. 571–590, 2014.

[3] J. G. Speight, *The Chemistry and Technology of Petroleum. Chemical Industries*. Boca Raton, FL: CRC Press, 2004.

[4] E. M. Ishiyama and S. J. Pugh, "Considering in-tube crude oil boiling in assessing performance of preheat trains subject to fouling," *Heat Transfer Eng.*, vol. 36, no. 7–8, pp. 632–641, 2015.

[5] E. M. Ishiyama, S. J. Pugh, B. Paterson, G. T. Polley, J. Kennedy, and D. I. Wilson, "Management of crude preheat trains subject to fouling," *Heat Transfer Eng.*, vol. 34, no. 8–9, pp. 692–701, 2013.

[6] S. Wauters and G. B. Marin, "Computer generation of a network of elementary steps for coke formation during the thermal cracking of hydrocarbons," *Chem. Eng. J.*, vol. 82, no. 1–3, pp. 267–279, 2001.

[7] S. C. K. De Schepper, G. J. Heynderickx, and G. B. Marin, "Modeling the coke formation in the convection section tubes of a steam cracker," *Ind. Eng. Chem. Res.*, vol. 49, no. 12, pp. 5752–5764, 2010.

[8] A. V. Mahulkar, G. J. Heynderickx, and G. B. Marin, "Simulation of the coking phenomenon in the superheater of a steam cracker," *Chem. Eng. Sci.*, vol. 110, pp. 31–43, 2014.

[9] S. C. K. De Schepper, G. J. Heynderickx, and G. B. Marin, "Coupled simulation of the flue gas and process gas side of a steam cracker convection section," *AIChE J.*, vol. 55, no. 11, pp. 2773–2787, 2009.

[10] G. H. Hu, B. F. Yuan, L. Zhang, J. L. Li, W. L. Du, and F. Qian, "Coupled simulation of convection section with dual stage steam feed mixing of an industrial ethylene cracking furnace," *Chem. Eng. J.*, vol. 286, pp. 436–446, 2016.

[11] P. Verhees *et al.*, "1D model for coupled simulation of steam cracker convection section with improved evaporation model," *Chemie Ingenieur Technik*, vol. 88, no. 11, pp. 1650–1664, 2016.

[12] A.-F. Chang, K. Pashikanti, and Y. A. Liu, "Characterization, physical and thermodynamic properties of oil fractions," in *Refinery Engineering*. Darmstadt and Germany: Wiley-VCH Verlag GmbH & Co. KGaA, 2012, pp. 155.

[13] S. C. K. De Schepper, G. J. Heynderickx, and G. B. Marin, "Modeling the evaporation of a hydrocarbon

feedstock in the convection section of a steam cracker," *Comput. Chem. Eng.*, vol. 33, no. 1, pp. 122–132, 2009.

[14] T. S. Wung, and C. J. Chen, "Finite analytic solution of convective heat transfer for tube arrays in cross-flow: part I-Flow Field analysis," *J. Heat Transfer*, vol. 111, no. 3, pp. 633–640, 1989.

[15] B. E. Launder, G. J. Reece, and W. Rodi, "Progress in development of a Reynolds-Stress turbulence closure," *J. Fluid Mechan.*, vol. 68, no. 03, pp. 537–566, 1975.

[16] F. W. Dittus, and L. M. K. Boelter, "Heat transfer in automobile radiator of the tubular type," *Int. Comm. Heat Mass Transfer*, vol. 2, no. 1, pp. 3–22, 1985.

[17] G. H. Hu, H. G. Wang, F. Qian, K. M. Van Geem, C. M. Schietekat, and G. B. Marin, "Coupled simulation of an industrial naphtha cracking furnace equipped with long-flame and radiation burners," *Comput. Chem. Eng.*, vol. 38, pp. 24–34, 2012.